Research Article | Vol. 25, No. 19 | 18 Sep 2017 | OPTICS EXPRESS 22911
Optics EXPRESS

Enhanced light emission from improved homogeneity in biaxially suspended Germanium membranes from curvature optimization

DANIEL BURT,[1] ABDELRAHMAN AL-ATTILI,[1] ZUO LI,[1] FRÉDÉRIC GARDÈS,[1] MOÏSE SOTTO,[1] NAOKI HIGASHITARUMIZU,[2] YASUHIKO ISHIKAWA,[2] KATSUYA ODA,[3] OSVALDO M. QUERIN,[4] SHINICHI SAITO,[1,*] AND ROBERT KELSALL[4]

[1]*Nanoelectronics & Nanotechnology Research Group, ZI, ECS, FPSE, Univ. of Southampton, UK*
[2]*Department of Materials Engineering, Graduate School of Engineering, The University of Tokyo, Tokyo, Japan*
[3]*Research & Development Group, Hitachi, Ltd., 1-280 Higashi-Koigakubo, Kokubunji, Tokyo 185-8601, Japan*
[4]*Institute of Microwaves and Photonics, School of Electronic & Electrical Engineering, University of Leeds, UK*
[*]*S.Saito@soton.ac.uk*

Abstract: A silicon compatible light source is crucial to develop a fully monolithic silicon photonics platform. Strain engineering in suspended Germanium membranes has offered a potential route for such a light source. However, biaxial structures have suffered from poor optical properties due to unfavorable strain distributions. Using a novel geometric approach and finite element modelling (FEM) structures with improved strain homogeneity were designed and fabricated. Micro-Raman (μ-Raman) spectroscopy was used to determine central strain values. Micro-photoluminescence (μ-PL) was used to study the effects of the strain profiles on light emission; we report a PL enhancement of up to 3x by optimizing curvature at a strain value of 0.5% biaxial strain. This geometric approach offers opportunity for enhancing the light emission in Germanium towards developing a practical on chip light source.

OCIS codes: (220.0220) Optical design and fabrication; (250.0250) Optoelectronics.

References and links

1. D. A. B. Miller, "Rationale and challenges for optical interconnects to electronic chips," Proc. IEEE **88**(6), 728–749 (2000).
2. R. Soref, "Mid-infrared photonics in silicon and germanium," Nat. Photonics **4**(8), 495–497 (2010).
3. G. Reed and A. Knights, *Silicon Photonics* (John Wiley, 2004).
4. K. Debnath, H. Arimoto, M. K. Husain, A. Prasmusinto, A. Al-Attili, R. Petra, H. M. H. Chong, G. T. Reed, and S. Saito, "Low-Loss Silicon Waveguides and Grating Couplers Fabricated Using Anisotropic Wet Etching Technique," Front. Mater. **3**, 10 (2016).
5. J. Michel, J. Liu, and L. C. Kimerling, "High-performance Ge on Si photodetectors," Nat. Photonics **4**(8), 527–534 (2010).
6. M. Cardona and F. H. Pollak, "Energy-Band Structure of Germanium and Silicon: The k·p method," Phys. Rev. **142**(2), 530–543 (1966).
7. S. Saito, F. Gardes, A. Al-Attili, K. Tani, K. Oda, Y. Suwa, T. Ido, Y. Ishikawa, S. Kako, S. Iwamoto, and Y. Arakawa, "Group IV Light Sources to Enable the Convergence of Photonics and Electronics," Front. Mater. **1**, 15 (2014).
8. S. Saito, A. Al-Attili, K. Oda, and Y. Ishikawa, "Towards monolithic integration of germanium light sources on silicon chips," Semicond. Sci. Technol. **31**(4), 043002 (2016).
9. J. Liu, X. Sun, L. C. Kimerling, and J. Michel, "Direct-gap optical gain of Ge on Si at room temperature," Opt. Lett. **34**(11), 1738–1740 (2009).
10. J. Liu, X. Sun, R. Camacho-Aguilera, L. C. Kimerling, and J. Michel, "Ge-on-Si laser operating at room temperature," Opt. Lett. **35**(5), 679–681 (2010).

#298079 https://doi.org/10.1364/OE.25.022911
Journal © 2017 Received 15 Jun 2017; revised 9 Aug 2017; accepted 11 Aug 2017; published 11 Sep 2017

Optics EXPRESS

11. R. E. Camacho-Aguilera, Y. Cai, N. Patel, J. T. Bessette, M. Romagnoli, L. C. Kimerling, and J. Michel, "An electrically pumped germanium laser," Opt. Express **20**(10), 11316–11320 (2012).
12. R. Geiger, T. Zabel, E. Marin, A. Gassenq, J. M. Hartmann, J. Widiez, J. Escalante, K. Guilloy, N. Pauc, D. Rouchon, G. Osvaldo Diaz, S. Tardif, F. Rieutord, I. Duchemin, Y. M. Niquet, V. Reboud, V. Calvo, A. Chelnokov, J. Faist, and H. Sigg, "Uniaxially stressed Germanium with fundamental direct band gap," arXiv **1603**, 03454 (2015).
13. M. El Kurdi, G. Fishman, S. Sauvage, and P. Boucaud, "Band structure and optical gain of tensile-strained germanium based on a 30 band k·p formalism," J. Appl. Phys. **107**(1), 013710 (2010).
14. O. Aldaghri, Z. Ikonić, and R. Kelsall, "Optimum strain configurations for carrier injection in near infrared Ge lasers," J. Appl. Phys. **111**(5), 053106 (2012).
15. Y. Ishikawa, K. Wada, D. Cannon, J. Liu, H. Luan, and L. Kimerling, "Strain-induced band gap shrinkage in Ge grown on Si substrate," J. Appl. Phys. **82**(13), 2044–2046 (2003).
16. G. Capellini, G. Kozlowski, Y. Yamamoto, M. Lisker, C. Wenger, G. Niu, P. Zaumseil, B. Tillack, A. Ghrib, M. de Kersauson, M. El Kurdi, P. Boucaud, and T. Schroeder, "Strain analysis in SiN/Ge microstructures obtained via Si-complementary metal oxide semiconductor compatible approach," J. Appl. Phys. **113**(1), 013513 (2013).
17. R. W. Millar, K. Gallacher, A. Samarelli, J. Frigerio, D. Chrastina, G. Isella, T. Dieing, and D. J. Paul, "Extending the emission wavelength of Ge nanopillars to 2.25 μm using silicon nitride stressors," Opt. Express **23**(14), 18193–18202 (2015).
18. A. Ghrib, M. El Kurdi, M. de Kersauson, M. Prost, S. Sauvage, X. Checoury, G. Beaudoin, I. Sagnes, and P. Boucaud, "Tensile-strained germanium microdisks," J. Appl. Phys. **102**(22), 221112 (2013).
19. M. El Kurdi, M. Prost, A. Ghrib, S. Sauvage, X. Checoury, G. Beaudoin, I. Sagnes, G. Picardi, R. Ossikovski, and P. Boucaud, "Direct Band Gap Germanium Microdisks Obtained with Silicon Nitride Stressor Layers," ACS Photonics **3**(3), 443–448 (2016).
20. A. Al-Attili, S. Kako, M. Husain, F. Gardes, S. Iwamoto, Y. Arakawa, and S. Saito, "Tensile strain engineering of germanium micro-disks on free-standing SiO_2 beams," Jpn. J. Appl. Phys. **55**(4S), 04EH02 (2016).
21. A. Al-Attili, S. Kako, M. Husain, F. Gardes, N. Higashitarumizu, S. Iwamoto, Y. Arakawa, Y. Ishikawa, H. Arimoto, K. Oda, T. Ido, and S. Saito, "Whispering Gallery Mode Resonances from Ge Micro-Disks on Suspended Beams," Front. Mater. **2**, 43 (2015).
22. J. R. Jain, A. Hryciw, T. M. Baer, D. A. B. Miller, M. L. Brongersma, and R. T. Howe, "A micromachining-based technology for enhancing germanium light emission via tensile strain," Nat. Photonics **6**(6), 398–405 (2012).
23. M. Süess, R. Geiger, R. Minamisawa, G. Schiefler, J. Frigerio, D. Chrastina, G. Isella, R. Spolenak, J. Faist, and H. Sigg, "Analysis of enhanced light emission from highly strained germanium microbridges," Nat. Photonics **7**(6), 466–472 (2013).
24. D. S. Sukhdeo, D. Nam, J. Kang, M. Brongersma, and K. Saraswat, "Direct bandgap germanium-on-silicon inferred from 5.7% ⟨100⟩ uniaxial tensile strain," Photon. Res. **2**(3), A8–A13 (2014).
25. D. Nam, D. S. Sukhdeo, J. H. Kang, J. Petykiewicz, J. H. Lee, W. S. Jung, J. Vučković, M. L. Brongersma, and K. C. Saraswat, "Strain-induced pseudoheterostructure nanowires confining carriers at room temperature with nanoscale-tunable band profiles," Nano Lett. **13**(7), 3118–3123 (2013).
26. H. Kroemer, "Quasi-Electric and Quasi-Magnetic Fields in Non-Uniform Semiconductors," RCA Review **18**, 332–342 (1957).
27. S. Ishida, S. Kako, K. Oda, T. Ido, S. Iwamoto, and Y. Arakawa, "Suspended germanium cross-shaped microstructures for enhancing biaxial tensile strain," Jpn. J. Appl. Phys. **55**(4S), 04EH14 (2016).
28. A. Gassenq, K. Guilloy, G. Osvaldo Dias, N. Pauc, D. Rouchon, J. Hartmann, J. Widiez, S. Tardif, F. Rieutord, J. Escalante, I. Duchemin, Y.-M. Niquet, R. Geiger, T. Zabel, H. Sigg, J. Faist, A. Chelnokov, V. Reboud, and V. Calvo, "1.9% bi-axial tensile strain in thick germanium suspended membranes fabricated in optical germanium-on-insulator substrates for laser applications," Appl. Phys. Lett. **107**(19), 191904 (2015).
29. D. S. Sukhdeo, S. Gupta, K. Saraswat, B. Dutt, and D. Nam, "Ultimate limits of biaxial tensile strain and n-type doping for realizing an efficient low-threshold Ge laser," Jpn. J. Appl. Phys. **55**(2), 024301 (2016).
30. D. S. Sukhdeo, D. Nam, J. H. Kang, M. L. Brongersma, and K. C. Saraswat, "Bandgap-customizable germanium using lithographically determined biaxial tensile strain for silicon-compatible optoelectronics," Opt. Express **23**(13), 16740–16749 (2015).
31. G. Capellini, G. Kozlowski, Y. Yamamoto, M. Lisker, C. Wenger, G. Niu, P. Zaumseil, B. Tillack, A. Ghrib, M. de Kersauson, M. El Kurdi, P. Boucaud, and T. Schroeder, "Strain analysis in SiN/Ge microstructures obtained via Si-complementary metal oxide semiconductor compatible approach," J. Appl. Phys. **113**(1), 013513 (2013).

1. Introduction

Silicon (Si) photonics could offer a solution to the traditional copper interconnect performance bottlenecks by replacing them with optical interconnects [1]. Furthermore, an on chip light source in the mid-infrared could pave the way for on chip bio/chemical sensing [2]. There has been much success in developing silicon compatible waveguides, modulators and detectors [3–5]. However, an efficient Si compatible light source has yet to be realized. Germanium (Ge) is a promising contender in developing such a light source due to its

Optics EXPRESS

epitaxial compatibility with Silicon, despite being an indirect bandgap material [6], which results in poor innate light emission due to phonon assisted photo radiative recombination. Ge can be converted into a direct bandgap material via the application of n-type doping and tensile strain [7–9]. An optically pumped Ge laser diode was reported at room temperature with 0.24% biaxial strain and 1 x 10^{-19}cm^{-3} *n*-type doping [10] as well as an electrically pumped laser with 4 x 10^{19} cm^{-3} n-type doping [11]. Despite these achievements, the threshold current densities were as high as 35 kA/cm^2 for optical pumping and 280kA/cm^2 for electrical pumping, for realization of a practical device the threshold current density must be drastically reduced. Dislocations act as non-radiative recombination centers degrading light emission, these dislocations are present due to the lattice mismatch during the epitaxial growth of Ge on Si.

Tensile strain offers a potential route to lowering threshold current density paving the way towards efficient practical devices. Ge can be converted into a direct bandgap material at a value of around 4.7% uniaxial tensile strain [12] and 1.9% biaxial strain [13,14]. There have been many practical methods developed for introducing high tensile strain into Ge. A small amount of biaxial strain is introduced in Ge when grown epitaxially on Silicon (Si) due to the difference in thermal expansion coefficients; this strain is usually around 0.15-0.25% [15]. While this strain can be a useful starting point, it is not enough to reduce threshold current density to a practical level. Other methods include depositing nitride stressor layers [16–19], suspending silicon dioxide and then transferring the strain into Ge micro disks [20,21] and suspending Germanium directly (the focus of this paper) [22–30].Suspended structures amplify the small amounts of tensile biaxial strain introduced during the epitaxial growth of Ge on Si. Certain regions of the Ge are suspended in which the membrane constricts resulting in an enhancement of the tensile strain, and the regions which are still tethered to the rest of the wafer (referred to as pads) relax resulting in a compressive strain. Suspension is generally achieved by dry etching 'windows' into the wafer and then using a wet etchant to under etch the substrate underneath thus suspending the Ge. By controlling the geometry of these etchant windows, both uniaxial and biaxial tensile strain can be introduced to the central region of the membrane [22].

Süess *et al* [23] recorded 3.1% uniaxial strain in a micro bridge geometry. Additionally strain induced pseudo-heterojunction effects resulted in the diffusion and subsequent confinement of carriers in the high strain region (due to a reduced direct bandgap), followed by subsequent recombination further enhancing light emission. Süess *et al* stated that the maximum achievable strain are limited by mechanical failure (cracking) of the membrane, usually caused by the point strain concentrations and dependent on the number of dislocations present in the Ge layer. Furthermore under etch length and profile were found to be extremely important parameters in enhancing the overall strain, theoretically the strain can be indefinitely enhanced with greater under etching provided as cracking is prevented. Sukhdeo *et al* suspended a Ge nanowire achieving an extremely large uniaxial strain of 5.7% enough to convert Ge into a direct band gap material [24]. Nam *et al* [25] reported a uniaxial suspended nanowire with a uniaxial tensile strain of 2.3% resulting in an inferred 200x PL intensity enhancement relative to bulk Ge. This was achieved utilizing strain induced double hetero-structures (s-DHs) and strain induced graded double hetero-structures (s-GDHs). s-DHs have a steep strain gradient confining the carriers along a uniform region whereas the s-GDHs have a gentle strain gradient forcing the carriers to the central active region due to quasi-electric fields [26]. s-GDHs are ideal for semiconductor lasers confining the carriers strongly and reducing the threshold current, applying a similar effect to compositionally graded hetero-junction laser diodes common for III-V materials without the need for hetero-epitaxy.

Following the success of uniaxial suspended Ge membranes, biaxial membranes were explored. Ishida *et al* developed a suspended Ge cross-shaped microstructure and optimized the pad lengths achieving 0.8% biaxial strain [27]; they achieved this using Ge on Si-on-insulator (SOI) this resulted in a 2.5X PL intensity enhancement. Gassenq *et al* fabricated Ge

Optics EXPRESS

membranes utilizing high quality GOI achieving a record high 1.9% biaxial strain, enough to convert Germanium into a direct band gap material [28]. Despite this extremely high strain, PL measurements were not possible due to strain induced redshifting beyond conventional detector cut off limit, thus the effect of this high strain on light emission is not clear. Furthermore, theoretical analysis shows that threshold optimization occurs at biaxial strain values of 3.7% and slope efficiency at 2.3% [29]. Sukhdeo *et al* also fabricated a monolithic slit based structures introducing up to 1.11% biaxial strain into Ge membranes utilizing GOI [30]. Despite high strain and good homogeneity, the observed increase in PL intensity was 2.4X opposed to a theoretically predicted 20X. This discrepancy was accredited to be due to the unfavorable strain profiles confining carriers to the highly strained corner regions acting as a parasitic mechanism reducing the observed PL intensity. Jain *et al* [22] used a combination on suspended Ge membranes as well as silicon nitride layers on the pads to enhance the strain reporting a large biaxial strain of 0.8% in an extremely large area of 40 μm^2. The observed PL enhancement was extremely large at 260 X likely due to the thermal effects and large area, the excited carriers cannot diffuse such great lengths and therefore the corner strain regions become inconsequential.

In this paper, we aimed to address the discrepancy between the theoretical and measured enhancement in light emission in biaxial Ge membranes by improving the homogeneity removing the high point corner strains. Biaxial membranes have suffered from poorer optical and mechanical properties compared to uniaxial. One main reason for this was homogeneity and in particular point stress concentrations, this work aimed to address this to improve homogeneity to make biaxial membranes a more viable option for light sources. We propose a novel geometric approach to explore the role of curvature on the strain distribution in an attempt to improve the strain homogeneity using finite element simulation. Devices were fabricated using a Ge on Si wafer stack. The structures were then characterized using μ-Raman spectroscopy to measure the central strain value and μ-PL to study the effect on light emission. By comparing the PL measurement with Raman spectroscopy and Finite Element Modelling (FEM), we confirmed that point strain concentrations were responsible for degrading the PL intensity. Curvature optimization is then required to improve homogeneity, which in turn improved light emission.

2. Design and simulation

2.1 Design

A unique geometric approach was employed to enhance the strain in the central area of the membrane whilst minimizing point strain concentrations whilst parametrically exploring the role of curvature. The structures are comprised of four arms, Fig. 1 Schematically shows how the half arm geometry was developed. The final four-armed geometry can be formed using copying, rotation and translation. The first step involves defining a geometric difference 'diff1' between a circular segment 'circ1' and square 'sq1' as shown in Fig. 1(a); this difference 'diff1' defines the curve at the extremity of the half arm. The square 'sq1' has dimensions that equal $L/2.4$ where L is arm length, its y position is fixed at 0 and the x positon (labelled 'r_{1x}') is given is also given in terms L, shown below as:

$$r_{1x} = L - (0.5(L / 2.4)) \tag{1}$$

Circular segment 'c_1' has its center at coordinates (0, 0) with a constant sector angle of 30°. The properties of 'sq_1' define the radius of the circular segment 'c_{1r}' as shown as:

$$c_{1r} = r_{1x} + (0.5 r_{1w}) \tag{2}$$

The second step involves defining the main bulk of the arm geometry. This step uses a circular segment 'circ2' as well as a rectangle (labelled r_1). The rectangle 'r_1' and the difference '$diff_1$' (defined in step 1) are subtracted from the circular segment circ2 as shown

Optics EXPRESS

in Fig. 1(b). The rectangle 'rect1' has a width equal to the arm length L and a height defined as H, furthermore it must be displaced in the y-axis by -H. Curvature ratio C can now be defined as

$$C = H / L \tag{3}$$

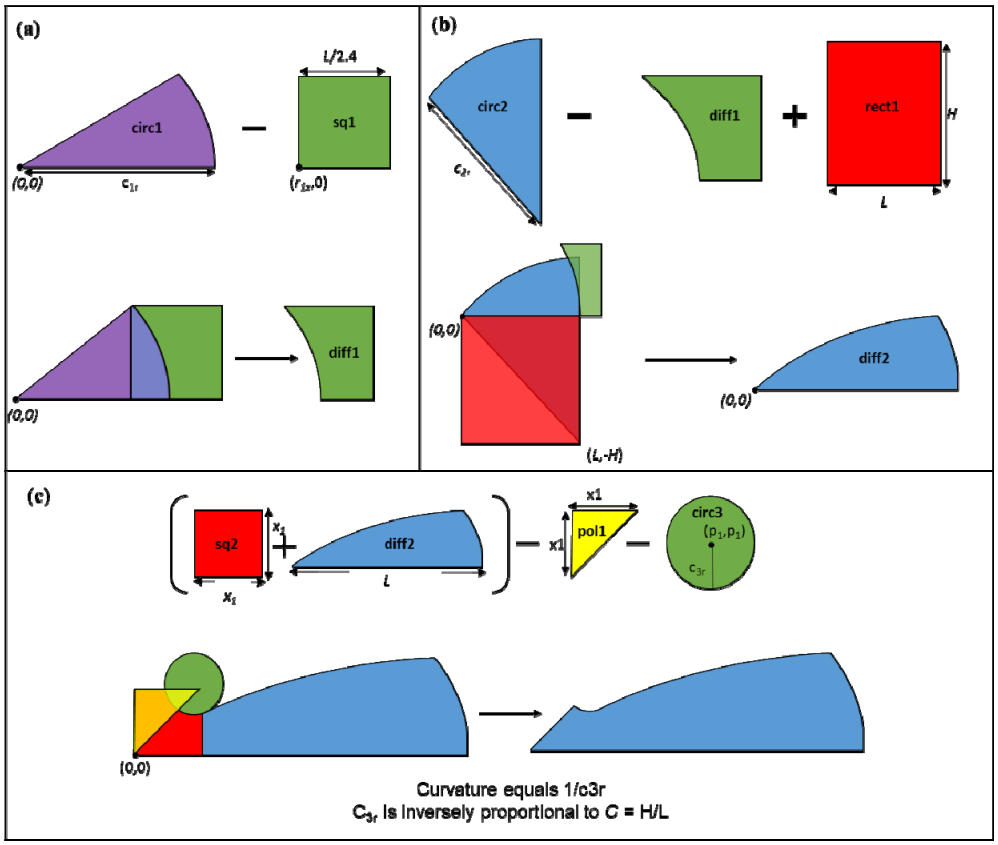

Fig. 1. Overall schematic of geometry design for half an arm with (a) Step 1 (b) Step 2 and (c) Step 3.

The circular segment circ2 is rotated 90 degrees and displaced in the x direction by L and in the y direction by – H. circ2 has a sector angle defined as gamma which is defined by an angle θ (note theta is not shown schematically for simplicity but shown mathematically). Circ2 has to have a radius c_{2r} shown in Fig. 1(b) and is given by:

$$c_{2r} = H / \cos(\gamma^o) \tag{4}$$

The value of C must be greater than unity otherwise the arc will over extend compromising the geometry. This is shown in Eq. (5) and Eq. (6) below:

$$\gamma = 90^o - \theta^o \tag{5}$$

$$\theta = \tan^{-1}(H / L) = \tan^{-1}(C) \tag{6}$$

The third step involves defining the curvature of the arm based on C achieved using a circle 'circ3′. A square labelled 'sq2' is added with its corner at (0, 0) and dimensions p_{2x} defined by Eq. (7) below with another required parameter p_{2y} defined as

Optics EXPRESS

$$p_{2x} = (L - (H / \cos(\gamma))(\cos(\theta + \beta)) \quad (7)$$

$$p_{2y} = ((H / \cos(\gamma))(\sin(\theta + \beta) - H) \quad (8)$$

Beta is an input parameter, which defines the central area, which for the purpose of this study is adjusted to give a fixed central circular area with diameter of 5.6 µm. P_1 defines the center coordinates of the circle circ3; it can be calculated by

$$P_1 = \frac{1}{2L} - \frac{(\sin(\gamma - \beta))(H + L)}{(\sin(135 - (\gamma - \beta)))} \quad (9)$$

To provide the curvature circ3 must be subtracted from the rest of the structure. The circle c_3 has central coordinates: (P_1, P_1) and radius 'c_{3r}', which is given by

$$c_{3r} = \sqrt{(p_{2x} - p_{1x})^2 + (p_{2y} - p_{1y})^2} \quad (10)$$

Finally, a polygon ('pol_1') is created to cut the structure at a 45° angle. After this, the half arm can be mirrored horizontally then copied and rotated to form the final four-armed structure. Furthermore, the curvature ratio can be altered resulting in varying geometries (as can be visualized in Fig. 2.

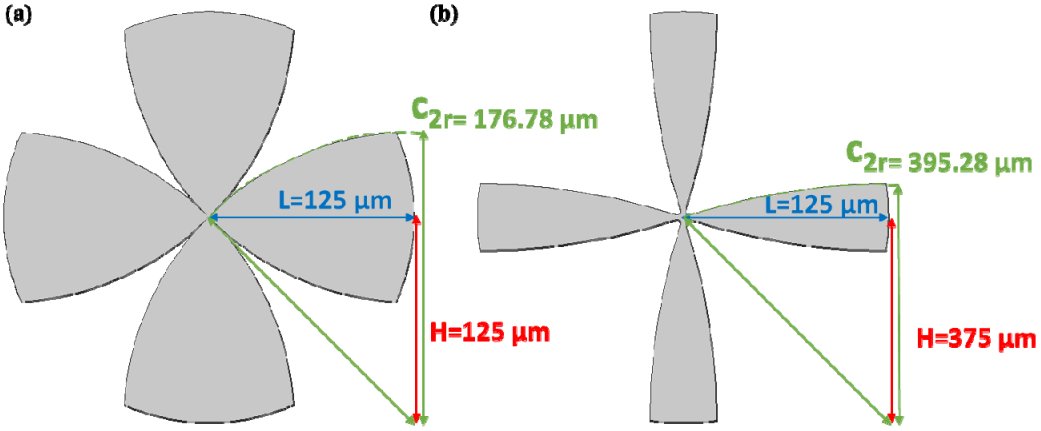

Fig. 2. Schematic of four arm structure with (a) C = 1.0 and (b) C = 3.0. The parameter L is fixed at 125 µm (shown in blue) and the corresponding parameters H (shown in red) and c_{2r} (shown in green).

2.2 Simulation

FEM using COMSOL Multiphysics v5.2 was used to study the strain homogeneity in the Ge membranes from C = *1.0* to C = 3.0 in increments of 0.2. The transport of dilute species model was used, assuming an isotropic diffusion to model the under-etchant profile fitted to a maximum etching distance of 25 µm. The structural mechanics module was then used assuming an initial strain of 0.18% in the membrane. The diffusion profiles were used to define a fixed constraint boundary condition. The central area had a fixed diameter of 5.6 µm. The central strain, maximum strain and the ratio between central and maximum strain were plotted as a function of C as shown in Fig. 3. Figure 3(a) shows the central strain decreases steadily as C increases; this is expected due to reduced pad size. This means the highest central strain values are in low C structures. However Fig. 3(b) shows the maximum strain is also largest at low C; the maximum strain rapidly decreases from C = 1.0 to C = 1.4 and then decreases slowly. The high corner strain concentrations degrade both optical and mechanical properties therefore these low C values are likely not suitable for practical applications.

Optics EXPRESS

Figure 3(c) shows the ratio between the central and maximum strain saturates at a value of around C = 1.8, at this point the largest central strain can be achieved whilst minimizing the maximum strain which in turn should increase resistance to plastic deformation and prevent detrimental carrier diffusion away from the central active region.

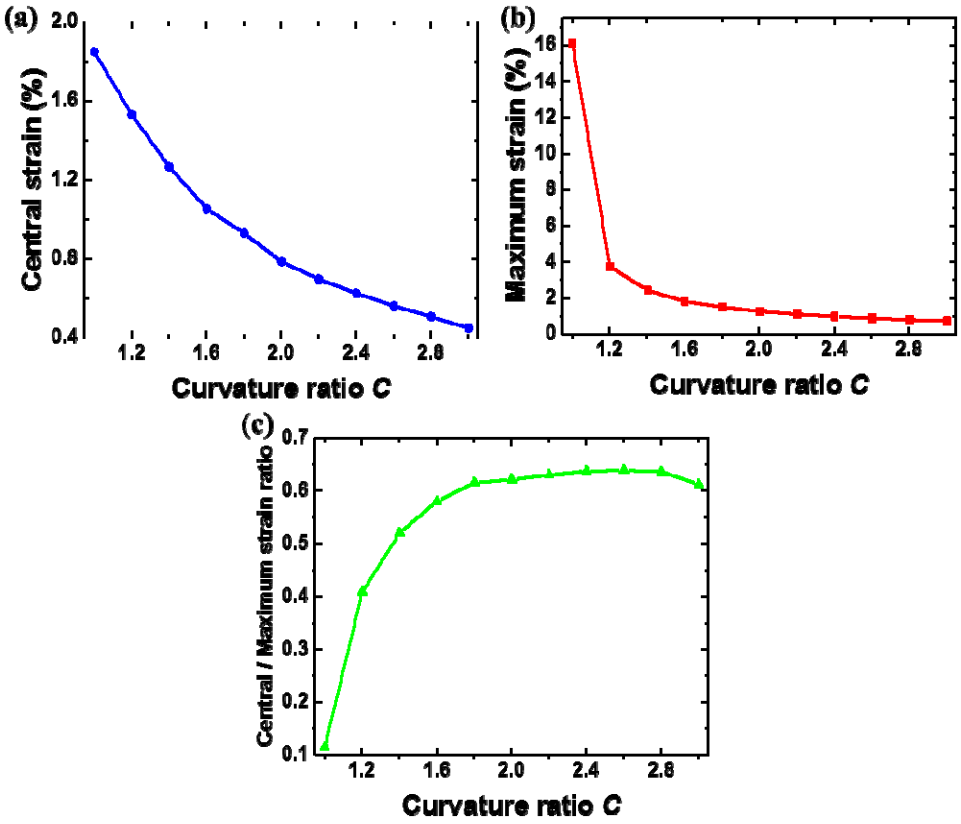

Fig. 3. The effect of *C* on (a) Central strain. (b) Maximum strain (c) The ratio between central and maximum strain.

Figure 4 shows the strain distributions at various *C* values. 2D simulations are sufficient as the depth of each membrane is identical, previous work [23] has shown that the tensile strain is maximum at the surface and decreases through the thickness. The tensile strain has been enhanced in the central region whilst compressive strain exist in the arms, as the force is constant in the membrane for the tensile enhancement in the central region to occur the arms must compress The maximum strain regions decrease in magnitude as *C* increases however they increase in size and shape, furthermore they migrate further from the central region as *C* increases. Figure 4(a) shows the strain distribution at *C* = 1.0, the maximum strain is concentrated in very small corner regions near the apex of the etchant windows in the central region. These extremely high point biaxial strain concentrations will likely cause mechanical failure (cracking or dislocation formation), furthermore optical properties may be degraded. Figure 4(b) shows the strain distribution at *C = 1.4*, the gradient between the maximum and the central strain is more gentle but these membranes are still likely to have poor optical and mechanical properties due to the high point strain concentrations.

Optics EXPRESS

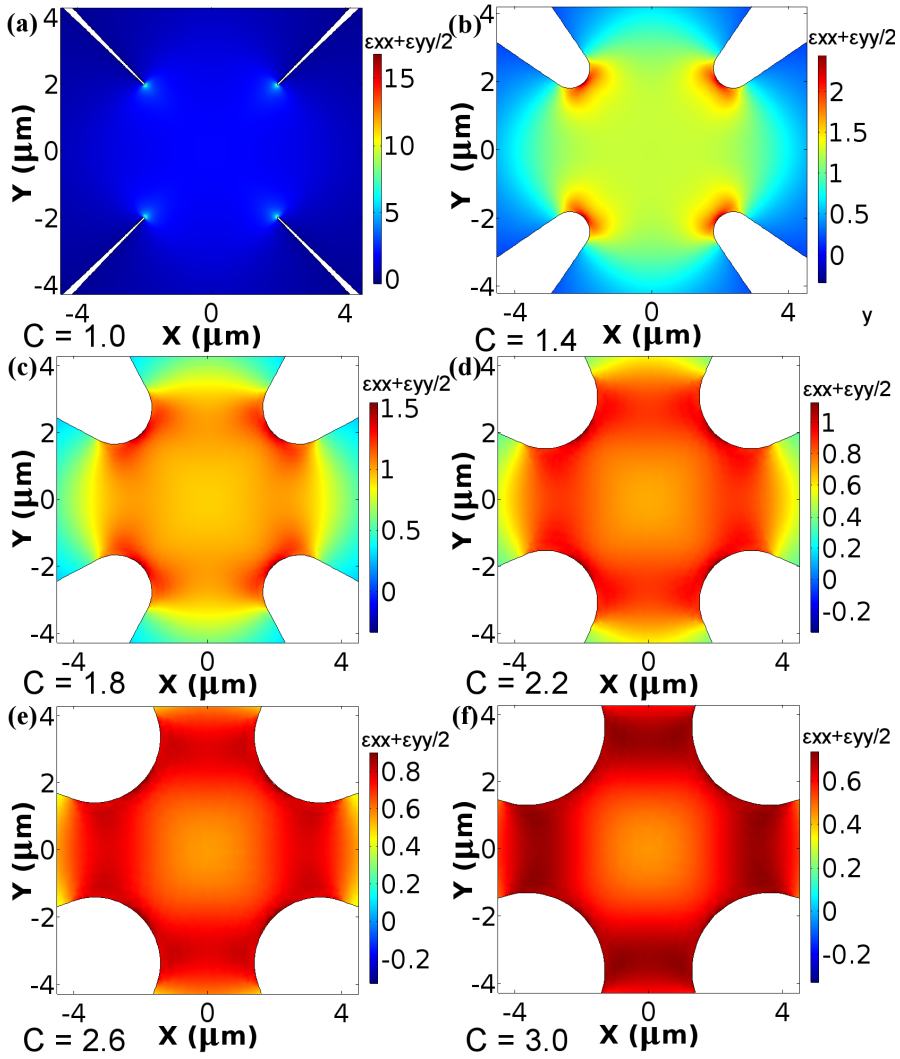

Fig. 4. Strain distributions at *C* values of (a) 1.0 (b) 1.4 (c) 1.8 (d) 2.2 (e) 2.6 and (f) 3.0.

Figure 4(c) shows the strain distribution at C = 1.8 which has a more gentle strain gradient and improved homogeneity. Figure 4(d) shows the strain distribution at *C* = 2.2, the homogeneity is very good at this point and the corner strain concentrations are much smaller. Figure 4(e) shows an interesting deviation from typical distributions in biaxial membranes exhibiting corner strains; the maximum strain begins to form into four rectangular regions just outside the main central region. In fact despite these regions having a higher value, the strain values are not purely biaxial and are asymmetric in nature, this reduces unfavorable carrier diffusion and subsequent recombination. Figure 4(f) shows the structure at C = 3.0, the maximum strain forms more distinct and stronger rectangular regions located outside the central regions in the arms. Structures with *C* > 2.6 show unique strain profiles, which deviate from previous works. These maximum strain regions highly asymmetric with varying contribution from the uniaxial strain components ϵ_{xx} and ϵ_{yy}. As the central strain is purely biaxial, a smaller strain value is required to reduce the direct bandgap relative to the corresponding uniaxial strain. In turn, the bandgap variation is not as large as the typical strain profiles in these structures with high corner strains (low *C* regime). With increasing C eventually the central region will become compressive in nature. Whilst the maximum strain

Optics EXPRESS

to minimum strain ratio is a good indication of homogeneity it is not a definition, the spatial strain profiles must also be considered in particular the size and location of the maximum strain regions. At higher C, the maximum regions are further away from the central region reducing pseudo-heterojunction effects. Furthermore they are less concentrated at the dry etched interfaces potentially minimizing surface non-radiative recombination and scattering.

3. Experimental

3.1 Fabrication

A Ge on Si wafer stack was chosen to fabricate the suspended membranes. The Ge layer was 532 nm thick, etching windows were patterned using electron beam lithography. This was followed by reactive ion etching (RIE) exposing the handle Si. Finally, a TMAH wet under-etch of the Si layer was performed resulting in an etching distance of 25 μm. Optical microscopy was used to observe the structures, from inspection it was noted that all of the low *C* structures were destroyed during fabrication (1.0 – 1.3) this was expected due to the high point strain concentrations. An optical micrograph of a surviving structure is shown in Fig. 5 corresponding to $C = 3.0$.

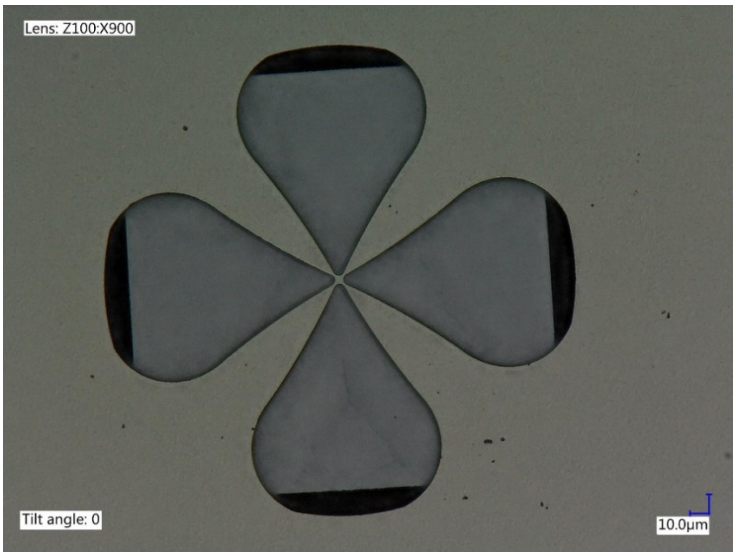

Fig. 5. Optical micrograph of successfully fabricated structure corresponding to C = 3.0.

3.2 Raman spectroscopy

Micro-Raman spectroscopy (μ-Raman) was performed to deduce the strain value in the central region of the structures. A green laser (532 nm wavelength) with a 100-x lens at a power of 100 μW resulting in a spot size with around a 1 μm diameter. Previous work from our group has determined the power dependency on the Raman peak position [20], a 100 μW power was used to make heating effects on the peak position negligible. Structures with *C* values of 1.4, 1.6, 1.8, 2.0, 2.5 and 3.0 to study the effect of curvature ratio (and thus curvature) on the strain. Figure 6(a) shows the μ-Raman spectra obtained. Structures $C \leq 1.3$ could not be used as none of them survived fabrication due to high point strain concentrations.

Optics EXPRESS

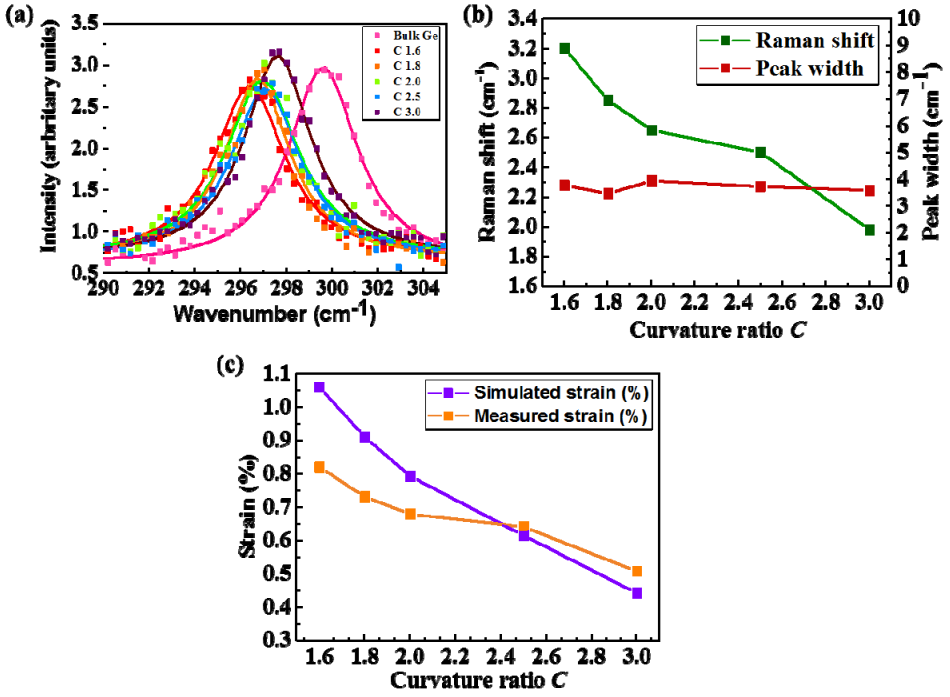

Fig. 6. (a) Raman spectra at various *C* values and bulk Ge (b) the Raman peak width and shift at various *C* values and (c) the extracted and simulated central strain values at various *C* values.

The peak shift and peak width were extracted from the Raman curves and plotted in Fig. 6(b). Raman shift decreases with increasing *C* that corresponds to decreasing strain as predicted due to lower pad size. The peak width remains relatively unchanged indicating that no substantial degradation of the crystalline quality has occurred. Figure 6(c) shows the measured strain values extracted from the peak shifts [31] using a proportionality factor of 390 cm^{-1} in addition to the corresponding simulated values, both show a trend of decreasing strain as *C* increases. The discrepancy between the simulated and measured values are likely due to an two dimensional isotropic etching profile being assumed during simulations whereas the fabricated devices have a more complex three dimensional anisotropic etching profile, however the strain distribution should not be effected by the anisotropic etching profile as the symmetry is the same.

3.3 Micro-photoluminescence (μ-PL) measurements

μ-PL measurements were conducted on the same structures as studied by μ-Raman spectroscopy. A green laser with a 532 nm wavelength was used to excite the central region of the structures with a power of 1.8 mW in conjunction with a 100-x lens resulting in a spot size of around 1 μm diameter at room temperature. Figure 7 shows the μ-PL spectra of structures with increasing *C* as well as bulk Ge as a reference. In general, complex spectra were produced with a broad emission profile; the spectra have been redshifted from the bulk Ge direct bandgap (corresponding to 1550 nm) due to the strain induced band gap reduction. The compressive strain fields in the arms cause the direct bandgap to increase in size and is likely the cause of the significant PL intensity below 1550 nm in the spectra. Furthermore, two distinct peaks appear in each spectra can be visualized likely due to light-hole (LH) and heavy-hole (HH) valence band splitting. Small Q factor modes can also be seen in some structures with the sharpest being in $C = 3.0$ likely originating from the longitudinal thickness

Optics EXPRESS

of the Ge membrane. It is difficult to ascertain where the μ-PL signal is coming from in the membrane using only a one-dimensional detector array, the spectra becomes complex due to central and maximum strain values as well as the subsequent LH and HH splitting, further work will be required to decouple these phenomena and locate the source of the μ-PL signal.

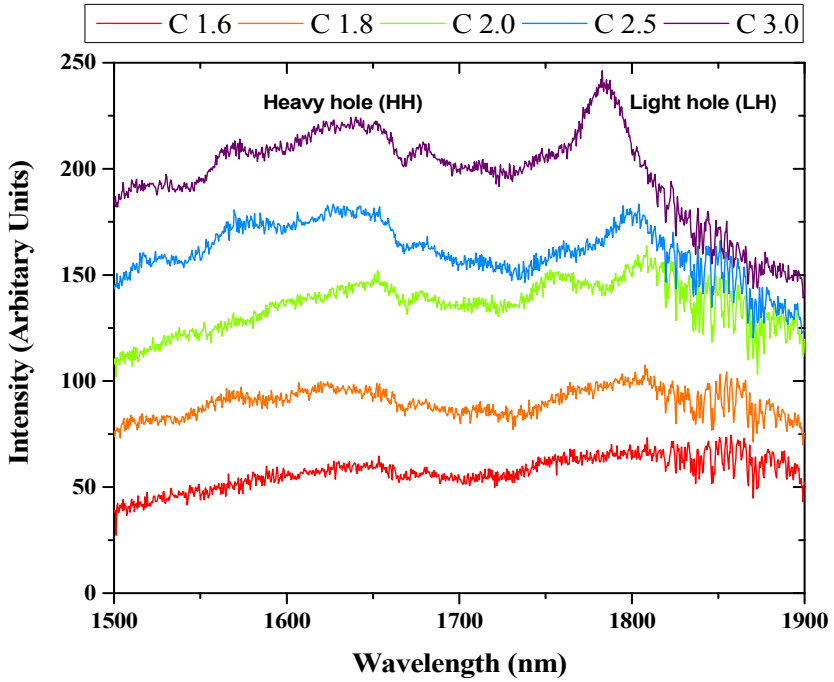

Fig. 7. μ-PL spectra of structures at increasing C. A cumulative y-offset of 25 was added to enable clear visualization of the spectra without overlap.

As *C* increases the intensity increases across the spectrum despite the strain decreasing. The intensity of the structure with *C* = 3.0 corresponding to a central strain of 0.52% has an enhancement of 3x relative to C = 1.6 at 1650nm. Thermal effects are an important issue in suspended membranes, as there is air either side of the membranes thickness, the heat cannot dissipate and the temperature of the membranes rise. The increase in temperature results in more indirect transitions and therefore enhanced PL signal as well as red shifting. However the heat dissipation in these membranes should be extremely similar due to similar lateral air gaps and therefore the thermal contribution cannot explain the enhanced PL intensity. One explanation for this enhancement could be due to dislocation formation at the low *C* structures due to higher strains; however, this is unlikely, as the peak width in the μ-Raman spectra, Fig. 6(b) remains relatively constant. Sukdeo *et al* reported a 2.4x PL enhancement in their biaxial suspended membranes [30] however, they had expected a 20x enhancement compared to bulk Germanium from theoretical calculations. One explanation provided for this discrepancy was pseudo-heterojunction carrier confinement effects occurring in the point strain concentrations in the corner of their structures (which were similar to low *C* structures). If the carriers were to recombine here, the emission could be redshifted past the detector limit and therefore not contribute to PL intensity. Another explanation for improved PL intensity at higher *C* could be due to a combination of carrier diffusion and surface recombination. In lower *C* structures the point stress accumulation occurs at the dry etched interface. If carriers diffuse towards this region with lower band gap, they could scatter or undergo non-radiative surface recombination both of which act as a potential loss mechanism. In higher *C* structures the maximum strain is further away and is not solely concentrated at the interface reducing

Optics EXPRESS

these potential losses. Further work is required to deduce the exact carrier behavior responsible for this PL enhancement.

4. Conclusion

By optimizing curvature and using FEM, structures with improved homogeneity were identified and improved light emission was confirmed by μ-PL studies. Structures with a high curvature (low C) exhibited large corner strain values, which were not present in the lower curvature (high C) structures. The lower curvature structures therefore had improved homogeneity, which was reflected in an enhanced μ-PL intensity in these structures despite lower central strain values. This study provides further evidence that high point strain values can be detrimental to both the mechanical and optical properties of biaxially suspended Ge membranes. This further highlights the need to consider the entire strain distribution when attempting to enhance light emission in Ge rather than absolute strain values. This geometric methodology can be applied to other strain platforms in Ge to enhance light emission not just suspended structures. Further work is required to understand the exact nature of the carrier dynamics responsible for enhanced light emission with improved homogeneity. A 3-x intensity enhancement from C = 1.6 to C = 3.0 was confirmed. With improved homogeneity, biaxially suspended Ge membranes become a more viable option as practical on chip light source.

Funding

This work is supported by EPSRC Manufacturing Fellowship (EP/M008975/1), EU FP7 Marie-Curie Carrier-Integration grant (PCIG13-GA-2013-61811), and EPSRC Institutional Sponsorship Research Collaboration. The data from the paper can be obtained from the University of Southampton e-Print research repository: http://doi.org/10.5258/SOTON/D0122.